Steel and Composite Structures, *Vol. 15, No. 2 (2013) 175-202*
DOI: http://dx.doi.org/10.12989/scs.2013.15.2.175

Super convergent laminated composite beam element for lateral stability analysis

Nam-Il Kim[1] and Dong-Ho Choi*[2]

[1] *Department of Architectural Engineering, Sejong University, 98 Kunja dong, Kwangin Ku, Seoul 143-747, Republic of Korea*
[2] *Department of Civil and Environmental Engineering, Hanyang University, 17 Haengdang-dong, Seongdong-Ku, Seoul, 133-791, Republic of Korea*

(Received March, 19, 2012, Revised April 11, 2013, Accepted June 27, 2013)

Abstract. The super convergent laminated composite beam element is newly derived for the lateral stability analysis. For this, a theoretical model of the laminated composite beams is developed based on the first-order shear deformation beam theory. The present laminated beam takes into account the transverse shear and the restrained warping induced shear deformation. The second-order coupling torque resulting from the geometric nonlinearity is rigorously derived. From the principle of minimum total potential energy, the stability equations and force-displacement relationships are derived and the explicit expressions for the displacement parameters are presented by applying the power series expansions of displacement components to simultaneous ordinary differential equations. Finally, the member stiffness matrix is determined using the force-displacement relationships. In order to show accuracy and superiority of the beam element developed by this study, the critical lateral buckling moments for bisymmetric and monosymmetric I-beams are presented and compared with other results available in the literature, the isoparametric beam elements, and shell elements from ABAQUS.

Keywords: stiffness matrix; lateral buckling; laminated composite beam; shear deformation

1. Introduction

The structural members made of composite materials are increasingly used in the fields of civil, mechanical, and aeronautical engineering applications, where high stiffness and strength, and low weight are of primary importance. The excellent fatigue characteristics in the direction of the fibers, corrosion resistance, and magnetic transparency are the main advantages of composite materials. A lot of structural members made of composite materials have the form of thin-walled cross-sections. These laminated composite beams might be subjected to the pure bending when used in above applications and are very susceptible to the lateral buckling. Therefore, the accurate prediction of their lateral stability limit state is of fundamental importance in the design of composite beams.

Up to the present, for the stability analysis of the laminated composite beams, the finite element method has been widely used because of its versatility and accordingly a large amount of work

*Corresponding author, Professor, E-mail: samga@hanyang.ac.kr

http://www.techno-press.org/?journal=scs&subpage=8 ISSN: 1229-9367 (Print), 1598-6233 (Online)

was devoted to the improvement of composite finite elements. Lee *et al*. (2002) performed the lateral stability analysis of the laminated composite beams with bisymmetric I-section. The displacement-based finite element model with 7 DOFs per node was developed. The generalized displacements were expressed over each element as a linear combination of the one-dimensional Lagrangian interpolation function and Hermite-cubic interpolation function. Lee (2006) studied the lateral buckling problem of the monosymmetric I-beams using the general geometrically nonlinear model based on the classical lamination theory. The theoretical model was developed by Cortínez and Piovan (2006) for the lateral stability analysis of composite thin-walled beams with general cross-sections. The model was presented using a non-linear displacement field, whose rotations were based on the rule of semi-tangential transformation, and the finite element with two-node and 14 DOFs was developed to solve the governing equations. Lin *et al*. (1996) developed the finite element stability analysis for a pultruded open section beam having 7 DOFs at each node by extending the study of Gunnlaugsson and Pedersen (1982). However, the main drawback of the above finite element analysis techniques is that a considerable number of finite elements are required to obtain the satisfactory results due to the use of the approximate shape functions.

In contrast to the finite element method, considerable research efforts to obtain analytical solutions for stability analysis of composite beams have been made by many researchers. Kollár and Springer (2003) and Sapkás and Kollár (2002) presented the solutions for the lateral buckling moments of the open section composite beams subjected to end moments. Vlasov's classical theory of the thin-walled beams was modified to consider the shear effects. Zhen and Wanji (2008) assessed several displacement-based theories by analyzing the buckling and free vibration behaviors of laminated beams with arbitrary layouts. Qiao *et al*. (2003) presented a combined analytical and experimental study of the flexural-torsional buckling of FRP composite cantilever I-beams. Three different type of buckling mode shapes of transcendental function, polynomial function, and half simply supported beam function were used to obtain the eigenvalue solutions. Kabir and Sherbourne (1998) presented the analytical solution for predicting the lateral buckling capacity of laminated beams including the influences of load form and lamination architecture. A detailed parametric study demonstrated that the improved design could be suggested which shows superior performance for optimal fiber orientation in both flanges and web in comparison with the traditional unidirected pultrusion process.

Another alternative numerical method to solve the buckling problems of composite beams is to develop the Ritz method. Machado and Cortínez (2005) developed a geometrically non-linear theory for thin-walled composite beams made of symmetric balanced laminates. The Ritz method was applied in order to solve the non-linear differential system. Shield and Morey (1997) presented a new theory for the stability analysis of composite beams that included the coupling effects caused by the Poisson effect using the Ritz method. They analyzed the I-section and box beams and showed that the inclusion of the anticlastic curvature substantially reduces the predicted buckling loads.

As a very effective approach in solving the stability and vibration problems of composite beams, the stiffness matrix method based on the solutions of the simultaneous ordinary differential equations was developed. The critical buckling loads and natural frequencies can be calculated using this method for any desired set of boundary conditions and assembly of elements. Abramovich *et al*. (1996) applied an exact element method to calculate the buckling loads and the natural frequencies of nonsymmetric laminated composite beams with rectangular cross-section. The influence of longitudinal and transverse restraints, material, and lay-up sequence on the buckling loads and natural frequencies of beam was investigated. Kim *et al*. (2007) evaluated the

exact element stiffness matrix in order to perform the spatially coupled stability analysis of thin-walled composite beams with symmetric and arbitrary lay-ups by using the eigenvelue problem. The exact displacement functions were constructed by combining eigenvectors and polynomial solutions corresponding to non-zero and zero eigenvalues. However, Kim *et al*. (2007) did not consider the effect of shear deformation. It is well known that for composite beams with low ratio of shear modulus to longitudinal modulus, the influence of shear strain on the stability of composite members is higher than that of the isotropic beams and must be accounted for in design. Piovan *et al*. (2008) employed a power series methodology to calculate the exact (or with arbitrary precision) free vibration frequencies of composite thin-walled tapered beams allowing for shear flexibility due to bending as well as non-uniform torsion warping. They investigated the effects of taper and the elastic couplings in the free vibration patterns of the beam.

The objective of this study is to present an improved analytical composite beam model and to calculate the lateral buckling moment exactly for the thin-walled composite beams considering the shear effects. A significant point of departure of the present numerical approach from other methods is in the solution of spatially coupled ordinary differential equations that arise in the solution process. Rather than using a discrete integration scheme or a finite element method based on energy principles, the present approach applies direct and systematic schemes for the evaluation of the element stiffness of the composite beams. The important points of this study are summarized as follows

1. The general linear theory is improved based on the orthogonal Cartesian coordinate system for the thin-walled laminated composite beams taking into account the transverse shear and the restrained warping induced shear deformation.
2. The geometrically nonlinear theory is developed for the stability analysis of the laminated composite beams. The second-order coupling torque (SOCT) which accounts for the change in the effective torsional stiffness due to the axial stress is rigorously derived.
3. The numerical method to evaluate the element stiffness matrix of shear deformable laminated composite beams with arbitrary lay-up is presented for lateral stability analysis.
4. For comparison, the finite beam element formulation based on the Lagrangian interpolation polynomials and the assumed displacement fields is presented to solve the lateral buckling problem for the laminated composite beams.
5. In order to demonstrate accuracy and superiority of this study, the critical lateral buckling moments of the bisymmetric and monosymmetric I-beams under the pure bending are evaluated and compared with the results from available references, the finite beam element, and shell elements from ABAQUS (2003).

2. General linear theory

2.1 Kinematics

In the present study, two coordinate systems which are mutually interrelated are used. The first coordinate system is the orthogonal Cartesian coordinate system (x, y, z), as shown in Fig. 1, where x axis is parallel to the longitudinal axis of the beam, while y and z are the principal axes of the cross-section having their origin at the shear center. The second coordinate system is the local coordinate system (x, n, s) for plate segment wherein n axis is normal to the middle surface of the

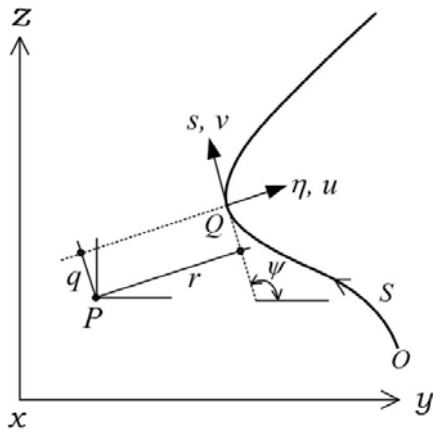

Fig. 1 Pictorial definitions of coordinates in thin-walled cross-section

plate, and the s axis is tangent to the middle surface and is directed along the contour line of the cross-section. The coordinates of an arbitrary point Q in the (x, n, s) coordinate system are (r, q), where r is the n coordinate and q is the s coordinate of Q. The ψ is the angle between the tangent to the contour and the y axis. The present structural model is based on the following assumptions.

1. The beam is prismatic and linearly elastic.
2. Each laminate is thin and perfectly bonded.
3. The cross-section is assumed to maintain its shape during deformation, so that there is no distortion.
4. The transverse shear and warping shear strains are incorporated. It is assumed that they are uniform over the cross-sections

Assuming that the cross-section is rigid with respect to the in-plane deformation and rotates about the shear center, the displacements of the arbitrary point on the cross-section can be expressed as (Kim *et al*. 1994)

$$\bar{u}(x,y,z) = u(x) - \omega_3(x)y + \omega_2(x)z + f(x)\phi \tag{1a}$$

$$\bar{v}(x,y,z) = v(x) - (z - e_3)\omega_1(x) \tag{1b}$$

$$\bar{w}(x,y,z) = w(x) + (y - e_2)\omega_1(x) \tag{1c}$$

where $u(x)$, $v(x)$, and $w(x)$ are the rigid body translations of the cross-section along the x, y, and z axes, respectively; $\omega_1(x)$, $\omega_2(x)$, and $\omega_3(x)$ are the rigid body rotations about the shear center and in the y and z axes, respectively; $f(x)$ is the parameter defining warping of the cross-section; e_2 and e_3 are coordinates of the pole P in the y and z axes, respectively; ϕ is the sectional property called the sectorial area or warping function. For the case of monosymmetic I-shaped section, it is defined as

$$\phi^{\alpha} = (z_{\alpha} - e_3)y \tag{2}$$

where the superscript α equals 1 and 2 for the top and bottom flanges, respectively; z_α is the z distance of the middle surface of each flange from the shear center.

In this formulation, owing to the effects of the flexural shear deformation, ω_2 and ω_3 are not equal to the derivatives of the corresponding translations. Similarly, f is not equal to the derivative of ω_1 owing to the inclusion of shear effect in warping. From the work of Kim *et al*. (1994), these rotations and warping parameter can be defined as

$$\omega_2 = \gamma_{xz}^o - w' \tag{3a}$$

$$-\omega_3 = \gamma_{xy}^o - v' \tag{3b}$$

$$f = \gamma_\phi^o - \omega_1' \tag{3c}$$

where γ_{xy}^o and γ_{xz}^o are the transverse shear strains due to flexure; γ_ϕ^o is the torsional shear strain associated with warping. The superscript 'prime' indicates the derivative with respect to x.

The buckling analysis of I-beams under bending, the deformation before buckling is ignored. The displacement components representing the deformation of any generic point in the top and bottom flanges can be expressed with respect to the middle surface displacements as

$$U^\alpha(x,y,z) = \bar{u}^\alpha(x,y) + \eta\frac{\partial w^\alpha}{\partial x}(x,y) \tag{4a}$$

$$V^\alpha(x,y,z) = \bar{v}^\alpha(x,y) + \eta\frac{\partial w^\alpha}{\partial y}(x,y) \tag{4b}$$

$$W^\alpha(x,y,z) = \bar{w}^\alpha(x,y) \tag{4c}$$

where $\bar{u}^\alpha$, $\bar{v}^\alpha$, and $\bar{w}^\alpha$ are the displacements of the middle surface of each flange. The displacement components for the web plate may also be expressed as

$$U^w(x,y,z) = \bar{u}^w(x,z) - \eta\frac{\partial v^w}{\partial x}(x,z) \tag{5a}$$

$$V^w(x,y,z) = \bar{v}^w(x,z) \tag{5b}$$

$$W^w(x,y,z) = \bar{w}^w(x,z) - \eta\frac{\partial v^w}{\partial z}(x,z) \tag{5c}$$

where $\bar{u}^w$, $\bar{v}^w$, and $\bar{w}^w$ are the displacements of the middle surface of the web.

The linear strain fields of the beam associated with the displacement fields of Eqs. (1), (4), and (5) can be expressed as

$$\varepsilon_x = \frac{\partial U}{\partial x} = \varepsilon_x^o + (z-\eta\cos\psi)\kappa_y + (y+\eta\sin\psi)\kappa_z + (\phi+\eta q)\kappa_\phi \tag{6a}$$

$$\gamma_{xy} = \frac{\partial U}{\partial y} + \frac{\partial V}{\partial x} = \gamma_{xy}^o - \gamma_\phi^o(z-e_3) + \kappa_{xs}\eta\cos\psi \tag{6b}$$

$$\gamma_{xz} = \frac{\partial U}{\partial z} + \frac{\partial W}{\partial x} = \gamma_{xz}^{o} + \gamma_{\phi}^{o}(y - e_2) + \kappa_{xs}\eta\sin\psi \tag{6c}$$

where γ_{xy}^{o}, γ_{xz}^{o} and γ_{ϕ}^{o} are flexural shear strains in the x_y and x_z planes and warping shear strain in the beam, respectively; ε_{x}^{o}, κ_{y}, κ_{z}, κ_{ϕ} and κ_{xs} are axial strain, biaxial curvatures in the y and z direction, warping curvature with respect to the shear center, and twisting curvature in the beam, respectively, defined as

$$\varepsilon_{x}^{o} = u', \quad \kappa_{y} = \omega_{2}', \quad \kappa_{z} = -\omega_{3}', \quad \kappa_{\phi} = f', \quad \kappa_{xs} = 2\omega_{1}' \tag{7}$$

2.2 Variational formulation

From the basic assumptions for the thin-walled beams (Barbero 1999), the linear strain energy of the laminated composite beam can be expressed as

$$\Pi_{L} = \frac{1}{2}\int_{V}\left(\sigma_{x}\varepsilon_{x} + \tau_{xy}\gamma_{xy} + \tau_{xz}\gamma_{xz}\right)dV \tag{8}$$

where σ_x, τ_{xy}, and τ_{xz} are normal and shear stresses, respectively. By substituting Eq. (6) into Eq. (8), the linear strain energy is expressed as

$$\begin{aligned}\Pi_{L} = \frac{1}{2}\int_{o}^{L}\int_{A}\Big[&\sigma_{x}\left\{\varepsilon_{x}^{o} + (z - \eta\cos\psi)\kappa_{y} + (y + \eta\sin\psi)\kappa_{z} + (\phi + \eta q)\kappa_{\phi}\right\} \\ &+ \tau_{xy}\left\{\gamma_{xy}^{o} - \gamma_{\phi}^{o}(z - e_3) + \kappa_{xs}\eta\cos\psi\right\} + \tau_{xz}\left\{\gamma_{xz}^{o} + \gamma_{\phi}^{o}(y - e_2) + \kappa_{xs}\eta\sin\psi\right\}\Big]dAdx\end{aligned} \tag{9}$$

where A and L are the area of cross-section and the length of beam, respectively. The variation of the linear strain energy in Eq. (9) can be written as

$$\delta\Pi_{L} = \int_{o}^{L}\left(F_1\delta\varepsilon_{x}^{o} + M_2\delta\kappa_{y} + M_3\delta\kappa_{z} + M_{\phi}\delta\kappa_{\phi} + T\delta\gamma_{\phi}^{o} + F_2\delta\gamma_{yx}^{o} + F_3\delta\gamma_{zx}^{o} + M_t\delta\kappa_{sx}\right)dx \tag{10}$$

where F_1 is the axial force; M_2 and M_3 are the bending moments about the y and z axes, respectively; M_ϕ is the bimoment; F_2 and F_3 are the shear forces in the y and z directions, respectively; T and M_t are the two contributions to the total twisting moment. These generalized forces and moments acting over the cross-section are related the stresses in the beam as

$$F_1 = \int_{A}\sigma_{x}\,dydz \tag{11a}$$

$$M_2 = \int_{A}\sigma_{x}(z - \eta\cos\psi)dydz \tag{11b}$$

$$M_3 = -\int_{A}\sigma_{x}(y + \eta\sin\psi)dydz \tag{11c}$$

$$M_{\phi} = \int_{A}\sigma_{x}(\phi + \eta q)dydz \tag{11d}$$

$$F_2 = \int_A \tau_{xy}\, dydz \tag{11e}$$

$$F_3 = \int_A \tau_{xz}\, dydz \tag{11f}$$

$$T = \int_A \left[\tau_{xz}(y - e_2) - \tau_{xy}(z - e_3)\right] dydz \tag{11g}$$

$$M_t = \int_A \left(\tau_{xy}\eta\cos\psi + \tau_{xz}\eta\sin\psi\right) dydz \tag{11h}$$

For the case of laminated composite material, the relationship between the plate stress tensors and the plate strain ones can be expressed in terms of the stiffness coefficients Q_{ij} of any constituent lamina of the beam wall. The stress-strain relationships of the kth lamina of the flanges are written in the Cartesian coordinate system as

$$\begin{Bmatrix} \sigma_x^f \\ \tau_{xy}^f \end{Bmatrix}^k = \begin{bmatrix} \overline{Q}_{11}^{*f} & \overline{Q}_{16}^{*f} \\ \overline{Q}_{16}^{*f} & \overline{Q}_{66}^{*f} \end{bmatrix}^k \begin{Bmatrix} \varepsilon_x^f \\ \gamma_{xy}^f \end{Bmatrix} \tag{12}$$

where $\overline{Q}_{ij}^{*}$ are the condensed stiffness coefficients of each lamina. The appropriate assumptions for constitutive relations are essential for a refined composite beam theory since the pile in the laminated composites behave in a highly two-dimensional manner due to the Poisson's effect (Smith and Chopra 1991). In this regard, the stress-strain relationships can be simplified by adopting the free stress ($\sigma_s = 0$) and the free strain ($\varepsilon_s = 0$) assumptions in contour direction. Thus for the free stress assumption, the condensed stiffness coefficients are given by

$$\overline{Q}_{11}^{*f} = \overline{Q}_{11} - \frac{\overline{Q}_{12}^2}{\overline{Q}_{22}} \tag{13a}$$

$$\overline{Q}_{16}^{*f} = \overline{Q}_{16} - \frac{\overline{Q}_{12}\overline{Q}_{26}}{\overline{Q}_{22}} \tag{13b}$$

$$\overline{Q}_{66}^{*f} = \overline{Q}_{66} - \frac{\overline{Q}_{26}^2}{\overline{Q}_{22}} \tag{13c}$$

where $\overline{Q}_{ij}$ are the transformed reduced stiffness coefficients (Barbero 1999) including the material properties of each lamina. For the free strain assumption, these are expressed as

$$\overline{Q}_{11}^{*f} = \overline{Q}_{11} \tag{14a}$$

$$\overline{Q}_{16}^{*f} = \overline{Q}_{16} \tag{14b}$$

$$\overline{Q}_{66}^{*f} = \overline{Q}_{66} \tag{14c}$$

Similarly, the constitutive equations for web are written as follows

$$\begin{Bmatrix} \sigma_x^w \\ \tau_{xz}^w \end{Bmatrix}^k = \begin{bmatrix} \overline{Q}_{11}^{*w} & \overline{Q}_{16}^{*w} \\ \overline{Q}_{16}^{*w} & \overline{Q}_{66}^{*w} \end{bmatrix}^k \begin{Bmatrix} \varepsilon_x^w \\ \gamma_{xz}^w \end{Bmatrix} \tag{15}$$

Substituting Eqs. (12) and (15) into Eq. (11), the constitutive equations for the laminated composite I-beams can be expressed as

$$\begin{Bmatrix} F_1 \\ M_2 \\ -M_3 \\ M_\phi \\ M_t \\ F_2 \\ F_3 \\ T \end{Bmatrix} = \begin{bmatrix} E_{11} & E_{12} & E_{13} & E_{14} & E_{15} & E_{16} & E_{17} & E_{18} \\ & E_{22} & E_{23} & E_{24} & E_{25} & E_{26} & E_{27} & E_{28} \\ & & E_{33} & E_{34} & E_{35} & E_{36} & E_{37} & E_{38} \\ & & & E_{44} & E_{45} & E_{46} & E_{47} & E_{48} \\ & & & & E_{55} & E_{56} & E_{57} & E_{58} \\ & & & & & E_{66} & E_{67} & E_{68} \\ & Symm. & & & & & E_{77} & E_{78} \\ & & & & & & & E_{88} \end{bmatrix} \begin{Bmatrix} u' \\ \omega_2' \\ -\omega_3' \\ f' \\ 2\omega_1' \\ v'-\omega_3 \\ w'+\omega_2 \\ \omega_1'+f \end{Bmatrix} \tag{16}$$

where E_{ij} are the laminate stiffnesses which depend on the cross-section of beam and detailed expressions are given in Appendix. Finally, substitution of Eq. (16) into Eq. (10) leads to the following linear strain energy of the shear deformable laminated composite I-beams.

$$\begin{aligned} \Pi_L = \frac{1}{2}\int_o^L \Big[& E_{11}u'^2 + E_{22}\omega_2'^2 + E_{33}\omega_3'^2 + E_{44}f'^2 + 4E_{55}\omega_1'^2 + E_{66}(v'-\omega_3)^2 + E_{77}(w'+\omega_2)^2 \\ & + E_{88}(\omega_1'+f)^2 + 2E_{12}u'\omega_2' - 2E_{13}u'\omega_3' + 2E_{14}u'f' + 4E_{15}u'\omega_1' + 2E_{16}u'(v'-\omega_3) \\ & + 2E_{17}u'(w'+\omega_2) + 2E_{18}u'(\omega_1'+f) - 2E_{23}\omega_2'\omega_3' + 2E_{24}\omega_2'f' + 4E_{25}\omega_1'\omega_2' + 2E_{26}\omega_2'(v'-\omega_3) \\ & + 2E_{27}\omega_2'(w'+\omega_2) + 2E_{28}\omega_2'(\omega_1'+f) - 2E_{34}\omega_3'f' - 4E_{35}\omega_1'\omega_3' - 2E_{36}\omega_3'(v'-\omega_3) \\ & - 2E_{37}\omega_3'(w'+\omega_2) - 2E_{38}\omega_3'(\omega_1'+f) + 4E_{45}\omega_1'f' + 2E_{46}f'(v'-\omega_3) + 2E_{47}f'(w'+\omega_2) \\ & + 2E_{48}f'(\omega_1'+f) + 4E_{56}\omega_1'(v'-\omega_3) + 4E_{57}\omega_1'(w'+\omega_2) + 4E_{58}\omega_1'(\omega_1'+f) \\ & + 2E_{67}(v'-\omega_3)(w'+\omega_2) + 2E_{68}(v'-\omega_3)(\omega_1'+f) + 2E_{78}(w'+\omega_2)(\omega_1'+f)\Big] dx \end{aligned} \tag{17}$$

3. Nonlinear strain energy

3.1 Nonlinear strain tensors

The nonlinear terms of the axial and shear strain fields are given by

$$\varepsilon_x^N = \frac{1}{2}\left[\left(\frac{\partial V}{\partial x}\right)^2 + \left(\frac{\partial W}{\partial x}\right)^2\right] \tag{18a}$$

$$\gamma_{xy}^N = \frac{\partial V}{\partial x}\frac{\partial V}{\partial y} + \frac{\partial W}{\partial x}\frac{\partial W}{\partial y} \tag{18b}$$

$$\gamma_{xz}^{N} = \frac{\partial V}{\partial x}\frac{\partial V}{\partial z} + \frac{\partial W}{\partial x}\frac{\partial W}{\partial z} \tag{18c}$$

Substituting Eqs. (1), (4), and (5) into Eq. (18), the nonlinear parts of the strains are written as follows

$$\begin{aligned}\varepsilon_{x}^{N} &= \frac{1}{2}\left[\left(\frac{\partial \overline{v}}{\partial x} + \eta\frac{\partial w}{\partial x \partial y}\right)^{2} + \left(\frac{\partial \overline{w}}{\partial x} - \eta\frac{\partial v}{\partial x \partial z}\right)^{2}\right] \\ &= \frac{1}{2}\Big[v'^{2} + w'^{2} + \omega_1'^{2}\left\{(y-e_2)^2 + (z-e_3)^2\right\} + \eta^2\omega_1'^{2} + 2\left\{w'\omega_1'(y-e_2) - v'\omega_1'(z-e_3)\right\} \\ &\quad + 2\eta\left\{v'\omega_1'\cos\psi + w'\omega_1'\sin\psi + \omega_1'^{2}(y-e_2)\sin\psi - \omega_1'^{2}(z-e_3)\cos\psi\right\}\Big]\end{aligned} \tag{19a}$$

$$\gamma_{xy}^{N} = w'\omega_1(\sin\psi + \cos\psi) + \omega_1\omega_1'(y-e_2)(\sin\psi + \cos\psi) + \eta\omega_1\omega_1'(\sin\psi\cos\psi + \sin^2\psi) \tag{19b}$$

$$\gamma_{xz}^{N} = -v'\omega_1(\sin\psi + \cos\psi) + \omega_1\omega_1'(z-e_3)(\sin\psi + \cos\psi) - \eta\omega_1\omega_1'(\sin\psi\cos\psi + \cos^2\psi) \tag{19c}$$

3.2 Variational formulation

The nonlinear strain energy of the laminated composite beam becomes

$$\Pi_N = \int_V \left(\sigma_x\varepsilon_x^{N} + \tau_{xy}\gamma_{xy}^{N} + \tau_{xz}\gamma_{xz}^{N}\right)dV \tag{20}$$

Substituting Eq. (19) into Eq. (20) and using the beam forces as given in Eq. (11), the nonlinear contribution of the strain energy expression can be expressed as

$$\begin{aligned}\Pi_N = \int_o^L \Big[&\frac{1}{2}{}^{o}F_1\left(v'^{2} + w'^{2} - 2e_2w'\omega_1' + 2e_3v'\omega_1'\right) - {}^{o}M_2v'\omega_1' - {}^{o}M_3w'\omega_1' \\ &+ {}^{o}F_2w'\omega_1 - {}^{o}F_3v'\omega_1 + \frac{1}{2}\Omega\omega_1'^{2}\Big]dx\end{aligned} \tag{21}$$

where the superscript '*o*' indicates the initial force variable and the stress resultant Ω denotes the second-order coupling torque (SOCT) term resulting from the geometric nonlinearity. This property is caused by the horizontal component of axial stress due to the inclination of the cross-section as a result of different warping. The twisting moment due to this will weaken the torsional rigidity if the axial stress is compressive. For the case of beam made of isotropic material, the above nonlinear strain energy is the same as the one in the study by Kim *et al*. (1994).

In order to derive the term Ω, the plate constitutive relations in the local coordinate system are considered as follows (Lee 2006)

$$\begin{Bmatrix}\overline{N}_x \\ \overline{N}_{xs} \\ \overline{M}_x \\ \overline{M}_{xs}\end{Bmatrix} = \begin{bmatrix} A_{11} & A_{16} & B_{11} & B_{16} \\ & A_{66} & B_{16} & B_{66} \\ & & D_{11} & D_{16} \\ symm. & & & D_{66}\end{bmatrix}\begin{Bmatrix}\overline{\varepsilon}_x \\ \overline{\gamma}_{xs} \\ \overline{\kappa}_x \\ \overline{\kappa}_{xs}\end{Bmatrix} \tag{22}$$

where $\overline{N}_x$, $\overline{N}_{xs}$, $\overline{M}_x$, and $\overline{M}_{xs}$ are plate stress resultants defined by

$$\left(\overline{N}_x, \overline{M}_x\right)=\int_\eta \sigma_x\left(1, \eta\right)d\eta \tag{23a}$$

$$\left(\overline{N}_{xs}, \overline{M}_{xs}\right)=\int_\eta \sigma_{xs}\left(1, \eta\right)d\eta \tag{23b}$$

In Eq. (22), $\overline{\gamma}_{xs}$ and $\overline{\kappa}_x$ are shear strain and axial curvature, respectively, in the middle surface of plate in local coordinate; A_{ij}, B_{ij} and D_{ij} are the extensional, bending-extension coupling, and bending stiffnesses, respectively, defined by

$$\left(A_{ij}, B_{ij}, D_{ij}\right)=\int_\eta \overline{Q}_{ij}^*\left(1, \eta, \eta^2\right)d\eta \tag{24}$$

From the study by Lee (2006), the term $\int_\eta \sigma_x\eta^2 d\eta$ in the nonlinear strain energy Eq. (21) can be written by

$$\begin{aligned}\int_\eta \sigma_x\eta^2 d\eta \;&=\; \int_\eta \left[\overline{Q}_{11}^*\left(\overline{\varepsilon}_x+\eta\overline{\kappa}_x\right)+\overline{Q}_{16}^*\left(\overline{\gamma}_{xs}+\eta\overline{\kappa}_{xs}\right)\right]\eta^2 d\eta \\ &= D_{11}\overline{\varepsilon}_x+H_{11}\overline{\kappa}_x+D_{16}\overline{\gamma}_{xs}+H_{16}\overline{\kappa}_{xs}\end{aligned} \tag{25}$$

where H_{ij}^* is the higher order stiffness given by

$$H_{ij}=\int_\eta \overline{Q}_{ij}^*\eta^3\, d\eta \tag{26}$$

From the plate constitutive relations in Eq. (22), Eq. (25) can be rewritten as

$$\int_\eta \sigma_x\eta^2 d\eta \;=\; \alpha_1\overline{N}_x+\alpha_2\overline{N}_{xs}+\alpha_3\overline{M}_x+\alpha_4\overline{M}_{xs} \tag{27}$$

where

$$\alpha_1 = D_{11}\beta_{11}+D_{16}\beta_{12}+H_{11}\beta_{13}+H_{16}\beta_{14} \tag{28a}$$

$$\alpha_2 = D_{11}\beta_{12}+D_{16}\beta_{22}+H_{11}\beta_{23}+H_{16}\beta_{24} \tag{28b}$$

$$\alpha_3 = D_{11}\beta_{13}+D_{16}\beta_{23}+H_{11}\beta_{33}+H_{16}\beta_{34} \tag{28c}$$

$$\alpha_4 = D_{11}\beta_{14}+D_{16}\beta_{24}+H_{11}\beta_{34}+H_{16}\beta_{44} \tag{28d}$$

In which β_{ij} are components of inverse matrix of Eq. (22) which is given by

$$\begin{bmatrix} \beta_{11} & \beta_{12} & \beta_{13} & \beta_{14} \\ & \beta_{22} & \beta_{23} & \beta_{24} \\ & & \beta_{33} & \beta_{34} \\ symm. & & & \beta_{44} \end{bmatrix} = \begin{bmatrix} A_{11} & A_{16} & B_{11} & B_{16} \\ & A_{66} & B_{16} & B_{66} \\ & & D_{11} & D_{16} \\ symm. & & & D_{66} \end{bmatrix}^{-1} \tag{29}$$

By using Eq. (27), the SOCT Ω can be expressed as follows

$$\Omega = \int_s \begin{bmatrix} \{(y-e_2)^2 + (z-e_3)^2 + \alpha_1\}\overline{N}_x + \alpha_2 \overline{N}_{xs} \\ + \{2(y-e_2)\sin\psi - 2(z-e_3)\cos\psi + \alpha_3\}\overline{M}_x + \alpha_4 \overline{M}_{xs} \end{bmatrix} ds \tag{30}$$

Substituting Eq. (22) into Eq. (30), Eq. (30) can be rewritten as follows

$$\Omega = E_{11}J_1\varepsilon_x^o + E_{22}J_2\kappa_y + E_{33}J_3\kappa_z + E_{44}J_4\kappa_\phi + E_{55}J_5\kappa_{xs} + E_{66}J_6\gamma_{xy}^o + E_{77}J_7\gamma_{xz}^o + E_{88}J_8\gamma_\phi^o \tag{31}$$

where

$$J_1 = \frac{1}{E_{11}}\int_s \begin{bmatrix} A_{11}\{(y-e_2)^2 + (z-e_3)^2 + \alpha_1\} + A_{16}\alpha_2 + \\ B_{11}\{2(y-e_2)\sin\psi - 2(z-e_3)\cos\psi + \alpha_3\} + B_{16}\alpha_4 \end{bmatrix} ds \tag{32a}$$

$$\begin{aligned} J_2 = \frac{1}{E_{22}}\int_s & \left[(A_{11}z - B_{11}\cos\psi)\{(y-e_2)^2 + (z-e_3)^2 + \alpha_1\} + (A_{16}z - B_{16}\cos\psi)\alpha_2 \right. \\ & \left. + (B_{11}z - D_{11}\cos\psi)\{2(y-e_2)\sin\psi - 2(z-e_3)\cos\psi + \alpha_3\} + (B_{16}z - D_{16}\cos\psi)\alpha_4\right] ds \end{aligned} \tag{32b}$$

$$\begin{aligned} J_3 = \frac{1}{E_{33}}\int_s & \left[(A_{11}y + B_{11}\sin\psi)\{(y-e_2)^2 + (z-e_3)^2 + \alpha_1\} + (A_{16}y + B_{16}\sin\psi)\alpha_2 \right. \\ & \left. + (B_{11}y + D_{11}\sin\psi)\{2(y-e_2)\sin\psi - 2(z-e_3)\cos\psi + \alpha_3\} + (B_{16}y + D_{16}\sin\psi)\alpha_4\right] ds \end{aligned} \tag{32c}$$

$$\begin{aligned} J_4 = \frac{1}{E_{44}}\int_s & \left[(A_{11}\phi - B_{11}q)\{(y-e_2)^2 + (z-e_3)^2 + \alpha_1\} + (A_{16}\phi - B_{16}q)\alpha_2 \right. \\ & \left. + (B_{11}\phi - D_{11}q)\{2(y-e_2)\sin\psi - 2(z-e_3)\cos\psi + \alpha_3\} + (B_{16}\phi - D_{16}q)\alpha_4\right] ds \end{aligned} \tag{32d}$$

$$J_5 = \frac{1}{E_{55}}\int_s \begin{bmatrix} B_{16}\{(y-e_2)^2 + (z-e_3)^2 + \alpha_1\} + B_{66}\alpha_2 \\ + D_{16}\{2(y-e_2)\sin\psi - 2(z-e_3)\cos\psi + \alpha_3\} + D_{66}\alpha_4 \end{bmatrix} ds \tag{32e}$$

$$\begin{aligned} J_6 = \frac{1}{E_{66}}\int_s & \left[A_{16}\cos\psi\{(y-e_2)^2 + (z-e_3)^2 + \alpha_1\} + A_{66}\cos\psi\alpha_2 \right. \\ & \left. + B_{16}\cos\psi\{2(y-e_2)\sin\psi - 2(z-e_3)\cos\psi + \alpha_3\} + B_{66}\cos\psi\alpha_4\right] ds \end{aligned} \tag{32f}$$

$$\begin{aligned} J_7 = \frac{1}{E_{77}}\int_s & \left[A_{16}\sin\psi\{(y-e_2)^2 + (z-e_3)^2 + \alpha_1\} + A_{66}\sin\psi\alpha_2 \right. \\ & \left. + B_{16}\sin\psi\{2(y-e_2)\sin\psi - 2(z-e_3)\cos\psi + \alpha_3\} + B_{66}\sin\psi\alpha_4\right] ds \end{aligned} \tag{32g}$$

$$\begin{aligned} J_8 = \frac{1}{E_{88}}\int_s & \left[A_{16}r\{(y-e_2)^2 + (z-e_3)^2 + \alpha_1\} + A_{66}r\alpha_2 \right. \\ & \left. + B_{16}r\{2(y-e_2)\sin\psi - 2(z-e_3)\cos\psi + \alpha_3\} + B_{66}r\alpha_4\right] ds \end{aligned} \tag{32h}$$

Now, the SOCT Ω can be expressed by using the constitutive equations in Eq. (16) of the laminated composite beam as

$$\Omega = \tilde{J}_1 F_1 + \tilde{J}_2 M_2 + \tilde{J}_3 M_3 + \tilde{J}_4 M_\phi + \tilde{J}_5 M_t + \tilde{J}_6 F_2 + \tilde{J}_7 F_3 + \tilde{J}_8 T \tag{33}$$

where

$$\left\{\tilde{J}_1 \;\; \tilde{J}_2 \;\; \tilde{J}_3 \;\; \tilde{J}_4 \;\; \tilde{J}_5 \;\; \tilde{J}_6 \;\; \tilde{J}_7 \;\; \tilde{J}_8\right\}^T = \mathbf{T}\left\{J_1 \;\; J_2 \;\; J_3 \;\; J_4 \;\; J_5 \;\; J_6 \;\; J_7 \;\; J_8\right\}^T \tag{34}$$

In Eq. (34), the transformed matrix **T** is expressed as follows

$$\mathbf{T} = \begin{bmatrix} E_{11}\delta_{11} & E_{22}\delta_{12} & E_{33}\delta_{13} & E_{44}\delta_{14} & E_{55}\delta_{15} & E_{66}\delta_{16} & E_{77}\delta_{17} & E_{88}\delta_{18} \\ E_{11}\delta_{12} & E_{22}\delta_{22} & E_{33}\delta_{23} & E_{44}\delta_{24} & E_{55}\delta_{25} & E_{66}\delta_{26} & E_{77}\delta_{27} & E_{88}\delta_{28} \\ -E_{11}\delta_{13} & -E_{22}\delta_{23} & -E_{33}\delta_{33} & -E_{44}\delta_{34} & -E_{55}\delta_{35} & -E_{66}\delta_{36} & -E_{77}\delta_{37} & -E_{88}\delta_{38} \\ E_{11}\delta_{14} & E_{22}\delta_{24} & E_{33}\delta_{34} & E_{44}\delta_{44} & E_{55}\delta_{45} & E_{66}\delta_{46} & E_{77}\delta_{47} & E_{88}\delta_{48} \\ E_{11}\delta_{15} & E_{22}\delta_{25} & E_{33}\delta_{35} & E_{44}\delta_{45} & E_{55}\delta_{55} & E_{66}\delta_{56} & E_{77}\delta_{57} & E_{88}\delta_{58} \\ E_{11}\delta_{16} & E_{22}\delta_{26} & E_{33}\delta_{36} & E_{44}\delta_{46} & E_{55}\delta_{56} & E_{66}\delta_{66} & E_{77}\delta_{67} & E_{88}\delta_{68} \\ E_{11}\delta_{17} & E_{22}\delta_{27} & E_{33}\delta_{37} & E_{44}\delta_{47} & E_{55}\delta_{57} & E_{66}\delta_{67} & E_{77}\delta_{77} & E_{88}\delta_{78} \\ E_{11}\delta_{18} & E_{22}\delta_{28} & E_{33}\delta_{38} & E_{44}\delta_{48} & E_{55}\delta_{58} & E_{66}\delta_{68} & E_{77}\delta_{78} & E_{88}\delta_{88} \end{bmatrix} \tag{35}$$

where δ_{ij} are the components of the inverse matrix of E_{ij} as

$$\begin{bmatrix} \delta_{11} & \delta_{12} & \delta_{13} & \delta_{14} & \delta_{15} & \delta_{16} & \delta_{17} & \delta_{18} \\ & \delta_{22} & \delta_{23} & \delta_{24} & \delta_{25} & \delta_{26} & \delta_{27} & \delta_{28} \\ & & \delta_{33} & \delta_{34} & \delta_{35} & \delta_{36} & \delta_{37} & \delta_{38} \\ & & & \delta_{44} & \delta_{45} & \delta_{46} & \delta_{47} & \delta_{48} \\ & & & & \delta_{55} & \delta_{56} & \delta_{57} & \delta_{58} \\ & & & & & \delta_{66} & \delta_{67} & \delta_{68} \\ & \textit{Symm.} & & & & & \delta_{77} & \delta_{78} \\ & & & & & & & \delta_{88} \end{bmatrix} = \begin{bmatrix} E_{11} & E_{12} & E_{13} & E_{14} & E_{15} & E_{16} & E_{17} & E_{18} \\ & E_{22} & E_{23} & E_{24} & E_{25} & E_{26} & E_{27} & E_{28} \\ & & E_{33} & E_{34} & E_{35} & E_{36} & E_{37} & E_{38} \\ & & & E_{44} & E_{45} & E_{46} & E_{47} & E_{48} \\ & & & & E_{55} & E_{56} & E_{57} & E_{58} \\ & & & & & E_{66} & E_{67} & E_{68} \\ & \textit{Symm.} & & & & & E_{77} & E_{78} \\ & & & & & & & E_{88} \end{bmatrix}^{-1} \tag{36}$$

On the other hand, the variation of the work done by external forces can be written as

$$\delta\Pi_{ext} = \delta \mathbf{U}_\mathbf{e}^\mathbf{T} \mathbf{F}_\mathbf{e} \tag{37}$$

where $\mathbf{U_e}$ and $\mathbf{F_e}$ denote the member end displacement and force vector, respectively.

In order to derive the stability equations and the force-displacement relationships of the laminated composite beam, the extended Hamilton's principle is used by

$$\int_{t_1}^{t_2} \delta\left(\Pi_L + \Pi_N - \Pi_{ext}\right) dt = 0 \tag{38}$$

Substituting Eqs. (17), (21), and (37) into Eq. (35) and integrating the derivatives of the varied quantities by parts, and collecting the coefficients of δu, δv, δw, $\delta\omega_1$, $\delta\omega_2$, $\delta\omega_3$, and δf, the stability equations are obtained as follows

$$E_{11}u'' + E_{16}v'' + E_{17}w'' + (2E_{15} + E_{18})\omega_1'' + E_{12}\omega_2'' + E_{17}\omega_2' - E_{13}\omega_3'' - E_{16}\omega_3' + E_{14}f'' + E_{18}f' = 0 \tag{39a}$$

$$E_{16}u'' + E_{66}v'' + E_{67}w'' + (2E_{56} + E_{68})\omega_1'' + E_{26}\omega_2'' + E_{67}\omega_2' - E_{36}\omega_3'' - E_{66}\omega_3' + E_{46}f'' + E_{68}f' + {}^oF_1(v'' + e_3\omega_1'') - {}^oM_2\omega_1'' - {}^oF_3\omega_1' = 0 \tag{39b}$$

$$E_{17}u'' + E_{67}v'' + E_{77}w'' + (2E_{57} + E_{78})\omega_1'' + E_{27}\omega_2'' + E_{77}\omega_2' - E_{37}\omega_3'' - E_{67}\omega_3' + E_{47}f'' + E_{78}f' + {}^oF_1(w'' - e_2\omega_1'') - {}^oM_3\omega_1'' + {}^oF_2\omega_1' = 0 \tag{39c}$$

$$\begin{aligned}(2E_{15} + E_{18})u'' + (2E_{56} + E_{68})v'' + (2E_{57} + E_{78})w'' + (4E_{55} + 4E_{58} + E_{88})\omega_1'' + (2E_{25} + E_{28})\omega_2'' \\ + (2E_{57} + E_{78})\omega_2' - (2E_{35} + E_{38})\omega_3'' - (2E_{56} + E_{68})\omega_3' + (2E_{45} + E_{48})f'' + (2E_{58} + E_{88})f' \\ - {}^oF_1(e_2w'' - e_3v'') - {}^oM_2v'' - {}^oM_3w'' - {}^oF_2w' + {}^oF_3v' + \Omega\omega_1'' = 0\end{aligned} \tag{39d}$$

$$E_{12}u'' - E_{17}u' + E_{26}v'' - E_{67}v' + E_{27}w'' - E_{77}w' + (2E_{25} + E_{28})\omega_1'' - (2E_{57} + E_{78})\omega_1' + E_{22}\omega_2'' - E_{77}\omega_2 - E_{23}\omega_3'' + (E_{37} - E_{26})\omega_3' + E_{67}\omega_3 + E_{24}f'' + (E_{28} - E_{47})f' - E_{78}f = 0 \tag{39e}$$

$$E_{13}u'' - E_{16}u' + E_{36}v'' - E_{66}v' + E_{37}w'' - E_{67}w' + (2E_{35} + E_{38})\omega_1'' - (2E_{56} + E_{68})\omega_1' + E_{23}\omega_2'' + (E_{37} - E_{26})\omega_2' - E_{67}\omega_2 - E_{33}\omega_3'' + E_{66}\omega_3 + E_{34}f'' + (E_{38} - E_{46})f' - E_{68}f = 0 \tag{39f}$$

$$E_{14}u'' - E_{18}u' + E_{46}v'' - E_{68}v' + E_{47}w'' - E_{78}w' + (2E_{45} + E_{48})\omega_1'' - (2E_{58} + E_{88})\omega_1' + E_{24}\omega_2'' + (E_{47} - E_{28})\omega_2' - E_{78}\omega_2 - E_{34}\omega_3'' + (E_{38} - E_{46})\omega_3' + E_{68}\omega_3 + E_{44}f'' - E_{88}f = 0 \tag{39g}$$

The seven force-displacement relationships can also be obtained as follows

$$F_1 = E_{11}u' + E_{16}v' + E_{17}w' + (2E_{15} + E_{18})\omega_1' + E_{17}\omega_2 + E_{12}\omega_2' - E_{16}\omega_3 - E_{13}\omega_3' + E_{18}f + E_{14}f' \tag{40a}$$

$$F_2 = E_{16}u' + (E_{66} + {}^oF_1)v' + E_{67}w' - {}^oF_3\omega_1 + (2E_{56} + E_{68} + {}^oF_1e_3 - {}^oM_2)\omega_1' + E_{67}\omega_2 + E_{26}\omega_2' - E_{66}\omega_3 - E_{36}\omega_3' + E_{68}f + E_{46}f' \tag{40b}$$

$$F_3 = E_{17}u' + E_{67}v' + (E_{77} + {}^oF_1)w' + {}^oF_2\omega_1 + (2E_{57} + E_{78} - {}^oF_1e_2 - {}^oM_3)\omega_1' + E_{77}\omega_2 + E_{27}\omega_2' - E_{67}\omega_3 - E_{37}\omega_3' + E_{78}f + E_{47}f' \tag{40c}$$

$$\begin{aligned}M_1 = (2E_{15} + E_{18})u' + (2E_{56} + E_{68} + {}^oF_1e_3 - {}^oM_2)v' + (2E_{57} + E_{78} - {}^oF_1e_2 - {}^oM_3)w' \\ + (4E_{55} + 4E_{58} + E_{88} + \Omega)\omega_1' + (2E_{57} + E_{78})\omega_2 + (2E_{25} + E_{28})\omega_2' \\ - (2E_{56} + E_{68})\omega_3 - (2E_{35} + E_{38})\omega_3' + (2E_{58} + E_{88})f + (2E_{45} + E_{48})f'\end{aligned} \tag{40d}$$

$$M_2 = E_{12}u' + E_{26}v' + E_{27}w' + (2E_{25} + E_{28})\omega_1' + E_{27}\omega_2 + E_{22}\omega_2' - E_{26}\omega_3 - E_{23}\omega_3' + E_{28}f + E_{24}f' \tag{40e}$$

$$M_3 = -E_{13}u' - E_{36}v' - E_{37}w' - (2E_{35} + E_{38})\omega_1' - E_{37}\omega_2 - E_{23}\omega_2' + E_{36}\omega_3 + E_{33}\omega_3' - E_{38}f - E_{34}f' \tag{40f}$$

$$M_\phi = E_{14}u' + E_{46}v' + E_{47}w' + (2E_{45} + E_{48})\omega_1' + E_{47}\omega_2 + E_{24}\omega_2' - E_{46}\omega_3 - E_{34}\omega_3' + E_{48}f + E_{44}f' \tag{40g}$$

If the cross-section is bisymmetric and the beam is made of the isotropic materials, in which the coupling effects are neglected, Eq. (39) can be simplified to the following uncoupled differential equations.

$$EAu'' = 0 \tag{41a}$$

$$GA_2(v'' - \omega_3') + {}^oF_1(v'' + e_3\omega_1'') - {}^oM_2\omega_1'' - {}^oF_3\omega_1' = 0 \tag{41b}$$

$$GA_3(w'' + \omega_2') + {}^oF_1(w'' - e_2\omega_1'') - {}^oM_3\omega_1'' + {}^oF_2\omega_1' = 0 \tag{41c}$$

$$GJ\omega_1'' + GA_r(\omega_1'' + f') - {}^oF_1(e_2w'' - e_3v'') - {}^oM_2v'' - {}^oM_3w'' - {}^oF_2w' + {}^oF_3v' - M_p\omega_1'' = 0 \tag{41d}$$

$$EI_2\omega_2'' - GA_3(w' + \omega_2) = 0 \tag{41e}$$

$$EI_3\omega_3'' + GA_2(v' - \omega_3) = 0 \tag{41f}$$

$$EI_\phi f'' - GA_r(\omega_1' + f) = 0 \tag{41g}$$

where E and G are the Young's modulus and the shear modulus, respectively; J is the St. Venant torsional constant and M_p is the stress resultant known as the Wagner effect and its detailed calculation procedure is given in the study of Kim *et al*. (1994); I_2, I_3, and I_ϕ are the second moments of inertia with respect to the y and z axes and the warping moment of inertia, respectively; A_2, A_3, and A_r are the effective shear areas defined according to the following expressions

$$\frac{1}{A_2} = \frac{1}{I_3^2}\int_A Z_3^2\frac{ds}{t},\quad \frac{1}{A_3} = \frac{1}{I_2^2}\int_A Z_2^2\frac{ds}{t},\quad \frac{1}{A_r} = \frac{1}{I_\phi^2}\int_A Z_r^2\frac{ds}{t} \tag{42}$$

where

$$Z_2 = \int_s ztds,\quad Z_3 = \int_s ytds,\quad Z_r = \int_s \phi tds \tag{43}$$

4. Stiffness matrix of laminated composite beam

4.1 Evaluation of displacement function

In order to derive the member stiffness matrix of the laminated composite beam, the displacement functions are rigorously evaluated based on the seven stability equations derived in Chapter 3. For this purpose, the seven displacement parameters are taken as the following infinite power series.

$$u = \sum_{n=0}^{\infty} a_n x^n,\quad v = \sum_{n=0}^{\infty} b_n x^n,\quad w = \sum_{n=0}^{\infty} c_n x^n$$
$$\omega_1 = \sum_{n=0}^{\infty} d_n x^n,\quad \omega_2 = \sum_{n=0}^{\infty} e_n x^n,\quad \omega_3 = \sum_{n=0}^{\infty} f_n x^n,\quad f = \sum_{n=0}^{\infty} g_n x^n \tag{44}$$

Substituting Eq. (44) into Eq. (39) and shifting the index of power of x^n, the stability equations can be compactly expressed in a matrix form as follows

$$\begin{aligned} &\{a_{n+2},\ b_{n+2},\ c_{n+2},\ d_{n+2},\ e_{n+2},\ f_{n+2},\ g_{n+2}\}^T \\ = \ &\mathbf{Z_n}\ \{a_n,\ a_{n+1},\ b_n,\ b_{n+1},\ c_n,\ c_{n+1},\ d_n,\ d_{n+1},\ e_n,\ e_{n+1},\ f_n,\ f_{n+1},\ g_n,\ g_{n+1}\}^T \end{aligned} \tag{45}$$

where $\mathbf{Z_n}$ is the 7×14 matrix function. The terms for a_{n+2}, b_{n+2}, c_{n+2}, d_{n+2}, e_{n+2}, f_{n+2} and g_{n+2} converge to zero as $n \to \infty$. We also define the initial integration constant vector **a** as

$$\mathbf{a} = \{a_o,\ a_1,\ b_o,\ b_1,\ c_o,\ c_1,\ d_o,\ d_1,\ e_o,\ e_1,\ f_o,\ f_1,\ g_o,\ g_1\}^T \tag{46}$$

The displacement state vector consisting of 14 displacement parameters is as follows

$$\mathbf{d} = \langle u,\ u',\ v,\ v',\ w,\ w',\ \omega_1,\ \omega_1',\ \omega_2,\ \omega_2',\ \omega_3,\ \omega_3',\ f,\ f' \rangle^T \tag{47}$$

The displacement state vector **d** can be expressed with respect to **a** by using Eqs. (44) and (45) as follows

$$\mathbf{d} \ = \ \mathbf{X_n}\ \mathbf{a} \tag{48}$$

where $\mathbf{X_n}$ denotes the 14×14 matrix function with the coefficients of u, v, w, ω_1, ω_2, ω_3, and f. In each of these 14 solution sets, the calculation of the coefficients by the recursive relations in Eq. (45) is continued until the contribution of the next coefficient is less than an arbitrarily chosen small number. Above symbolic calculations are performed with the help of the technical computer software Mathematica (2009).

Next, let $\mathbf{U_e}$ be the generalized nodal displacement vector having 14 DOFs at two ends of the beam element as shown in Fig. 2(a).

$$\begin{aligned} \mathbf{U_e} = \langle &u(0)\,,\ v(0)\,,\ w(0),\ \ \omega_1(0)\,,\ \omega_2(0)\,,\ \omega_3(0)\,,\ f(0) \\ &u(L)\,,\ v(L)\,,\ w(L),\ \ \omega_1(L)\,,\ \omega_2(L)\,,\ \omega_3(L)\,,\ f(L) \rangle^T \end{aligned} \tag{49}$$

Substituting coordinates of the two ends of member (x = 0, L) into Eq. (48), the nodal displacement vector $\mathbf{U_e}$ is expressed in terms of **a** as follows

$$\mathbf{U_e} \ = \ \mathbf{H}\ \mathbf{a} \tag{50}$$

From Eqs. (48) and (50), the displacement state vector **d** at an arbitrary point of element can be expressed with respect to the nodal displacement vector $\mathbf{U_e}$.

$$\mathbf{d} \ = \ \mathbf{X_n}\ \mathbf{H}^{-1}\ \mathbf{U_e} \tag{51}$$

It is noted that $\mathbf{X_n H}^{-1}$ in Eq. (51) is the exact shape function matrix since the displacement state vector **d** satisfies the homogenous form of the coupled equilibrium equations in Eq. (39) exactly.

4.2 Calculation of stiffness matrix

By using the displacement state vector **d** derived in previous section, the stiffness matrix of the laminated composite beam is rigorously calculated. The nodal force vector $\mathbf{F_e}$ at two ends p and q of the element as shown in Fig. 2(b) is considered as follows

$$\mathbf{F_e} = \left\langle \mathbf{F}^p , \mathbf{F}^q \right\rangle^T \tag{52}$$

where

$$\mathbf{F}^\xi = \left\langle F_1^\xi, F_2^\xi, F_3^\xi, M_1^\xi, M_2^\xi, M_3^\xi, M_\phi^\xi \right\rangle^T \quad , \quad \xi = p , q \tag{53}$$

The force-displacement relationships in Eq. (40) can be written as a matrix form

$$\mathbf{f(x)} = \mathbf{S\,d} \tag{54}$$

where **S** is the 7×14 matrix. Substitution of Eq. (51) into Eq. (54) leads to

$$\mathbf{f(x)} = \mathbf{S\,X_n\,H^{-1}\,U_e} \tag{55}$$

Now, the nodal forces at two ends of element are evaluated as

$$\mathbf{F}^p = -\mathbf{f}(0) = -\mathbf{S\,X_n}(0)\,\mathbf{H^{-1}\,U_e} \tag{56a}$$

$$\mathbf{F}^q = \mathbf{f}(L) = \mathbf{S\,X_n}(L)\,\mathbf{H^{-1}\,U_e} \tag{56b}$$

Finally, for the lateral stability analysis of the laminated composite beams, the element stiffness matrix is obtained based on the linear relation between member forces and nodal displacement parameters as follows

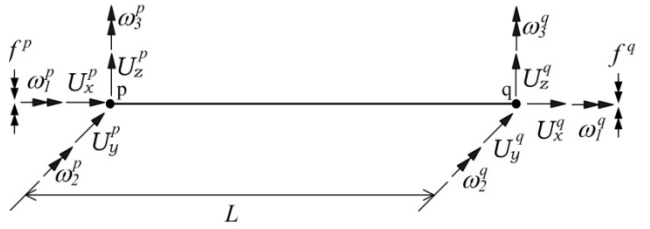

(a) Nodal displacements

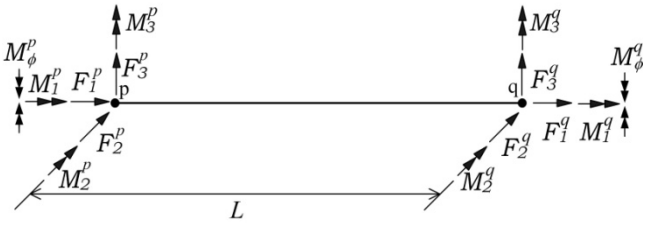

(b) Nodal forces

Fig. 2 Nodal displacements and forces of the laminated composite beam elements

$$\mathbf{F_e} = \mathbf{K}\,\mathbf{U_e} \tag{57}$$

where

$$\mathbf{K} = \begin{bmatrix} -\mathbf{S}\,\mathbf{X_n}(\mathbf{0})\mathbf{H}^{-1} \\ \mathbf{S}\,\mathbf{X_n}(\mathbf{l})\mathbf{H}^{-1} \end{bmatrix} \tag{58}$$

The critical buckling moments of the beam are the values that cause the stiffness matrix to become singular as Eq. (59). A search procedure is employed to find these values up to the desired accuracy. In this study, the Regular-Falsi method (Wendroff 1966) is applied to ensure that none of the buckling loads is missed.

$$|\mathbf{K}| = 0 \tag{59}$$

It is noteworthy that the stiffness matrix in Eq. (58) is formed by the shape functions which are exact solutions of the governing equations. Therefore, the thin-walled laminated composite beam using the stiffness matrix developed by this study eliminates discretization errors and is free from the shear and membrane locking.

For comparison, the finite beam element model with 7 DOFs per node is presented based on the Lagrangian interpolation polynomials. The present finite beam element uses the same shape functions for all translational, rotational, and warping displacements. The displacements can be expressed as follows

$$\begin{aligned} u &= \sum_{\alpha=1}^{2} N_\alpha u_\alpha, \quad v = \sum_{\alpha=1}^{2} N_\alpha v_\alpha, \quad w = \sum_{\alpha=1}^{2} N_\alpha w_\alpha, \\ \omega_i &= \sum_{\alpha=1}^{2} N_\alpha \omega_{i\alpha} \quad (i = 1, 2, 3), \quad f = \sum_{\alpha=1}^{2} N_\alpha f^\alpha \end{aligned} \tag{60}$$

where N_α is the Lagrangian interpolation function corresponding to node α, whose detailed expression is presented in Bathe (1996).

The nodal point displacement vector $\mathbf{U}_{f\alpha}$ and the element displacement vector $\mathbf{U}_{fe}$ can be defined as follows

$$\mathbf{U}_{f\alpha} = \left[u,\ v,\ w,\ \omega_1,\ \omega_2,\ \omega_3,\ f\right]^T \tag{61a}$$

$$\mathbf{U}_{fe} = \left[\mathbf{U}_1,\ \mathbf{U}_2\right]^T \tag{61b}$$

Similarly, the nodal force vector $\mathbf{F}_{f\alpha}$ and the element force vector $\mathbf{F}_{fe}$ can also be defined as follows

$$\mathbf{F}_{f\alpha} = \left[F_1,\ F_2,\ F_3,\ M_1,\ M_2,\ M_3,\ M_\phi\right]^T \tag{62a}$$

$$\mathbf{F}_{fe} = \left[\mathbf{F}_1,\ \mathbf{F}_2\right]^T \tag{62b}$$

Substituting the shape functions of Eq. (60) into the extended Hamilton's principle of Eq. (38), the element elastic stiffness matrix $\mathbf{k}^e$ and the element geometric stiffness matrix $\mathbf{k}^g$ can be obtained. The two stiffness matrices are evaluated using a reduced Gauss numerical integration scheme to alleviate shear locking.

Once each $\mathbf{k}^e$ and $\mathbf{k}^g$ of the element are assembled into $\mathbf{K}^E$ and $\mathbf{K}^G$ of the structures, the linearized buckling problem can be written as

$$\left(\mathbf{K}^E + \lambda \mathbf{K}^G\right)\mathbf{U} = \mathbf{0} \tag{63}$$

where λ is the buckling moment parameter under the assumption of proportional loading. The critical buckling moment is now obtained by solving Eq. (63) for the unknown eigenvalue λ using a shifted inverse iteration algorithm. The buckling moment is then found by multiplying the smallest eigenvalue λ by the applied moment.

5. Numerical examples

In order to demonstrate accuracy and superiority of the present laminated composite beam theory and the numerical method developed by this study, the coupled lateral buckling analysis has been performed for the bisymmetric and monosymmetric I-beams subjected to two equal and opposite end moments about strong axis. The results obtained from this study are compared with those from other researchers and the finite element solutions using the finite beam elements and the shell elements by ABAQUS.

5.1 Bisymmetric I-beams

The simply supported (SS) and orthotropic I-beams with bisymmetric cross-section are considered. The geometric properties of the cross-section, as shown in Fig. 3, are as follows: L = 10.0 m, $b_1 = b_2 = 102$ mm, $h = 241$ mm, $t_1 = t_2 = 16$ mm, and $t_3 = 9$ mm. The critical lateral buckling moments by this study using only one element are presented in Table 1 for various E_1 / G_{12} ratios ($E_1 = 17.225$ GPa) where subscripts '1' and '2' correspond to directions parallel and perpendicular to fibers, respectively. Here, for an isotropic material with the Poisson's ratio equal to 0.3, the E_1 / G_{12} ratio is 2.6. For the purpose of comparison, the finite element solutions from Lee *et al*. (2002)

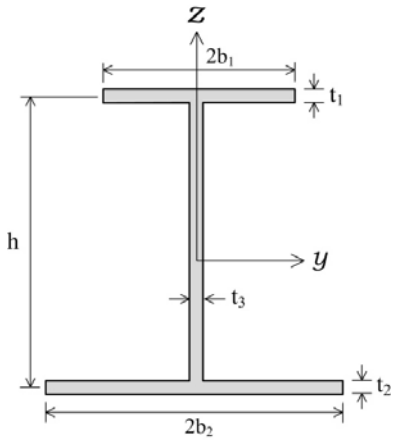

Fig. 3 Shape of cross-section under consideration

Table 1 Lateral buckling moments of the orthotropic SS beams with bisymmetric cross-section (kNm)

E_1 / G_{12}	This study		Lee *et al*. (2002)	Lin *et al*. (1996)
	$\sigma_s = 0$	$\varepsilon_s = 0$		
2.6	13.36	14.09	13.30	13.50
5.2	9.99	10.59	9.94	10.15
10	7.88	8.40	7.90	8.06
20	6.45	6.92	6.38	6.66
40	5.58	6.03	5.50	5.83

and Lin *et al*. (1996) are presented.

It can be found from Table 1 that the present solutions applying $\sigma_s = 0$ assumption are in good agreement with results in Lee *et al*. (2002) and Lin *et al*. (1996) for all ranges of E_1 / G_{12}. When the E_1 / G_{12} ratio increases from 2.6 to 40, the buckling moment decreases by about 58.2%. This reduction indicates that the shear strain plays a significant role on the lateral buckling capacity of the orthotropic I-beams.

The next example is the bisymmetric I-beams made with graphite-epoxy (AS4/3501) material with following material constants: $E_1 = 144$ GPa, $E_2 = E_3 = 9.65$ GPa, $G_{12} = G_{13} = 4.14$ GPa, $G_{23} = 3.45$ GPa, $v_{12} = v_{13} = 0.3$, and $v_{23} = 0.5$. The total 16 layers with equal thickness are symmetrically laminated with respect to the middle plane of flanges and web, and the sectional properties are as follows: $b_1 = b_2 = 25$ mm, $h = 50$ mm, $t_1 = t_2 = 2.08$ mm, and $t_3 = 3.20$ mm.

The critical lateral buckling moments of the clamped-free (CF) and simply supported (SS) beams with $L/h = 40$ from this study are presented and compared with results from various numbers of the finite beam elements, and those from ABAQUS for several stacking sequences. For ABAQUS calculation, a total of 480 nine node shell elements (S9R5) (80 along the beam span and 6 through the cross-section) are used. It is found from Tables 2 and 3 that the solutions from this study based on $\sigma_s = 0$ assumption are in good agreement with results from ABAQUS for all lay-ups considered. The analysis based on $\varepsilon_s = 0$ assumption overestimates the buckling moments by maximum 74.6% and 78.9% for CF and SS beams, respectively, at $\psi = 45°$. For results from the finite beam elements, as a number of beam element increases, its solutions converge to

Table 2 Lateral buckling moments of CF beams with bisymmetric cross-section (Nm)

Lay-ups	Number of finite beam elements, $\sigma_s = 0$					This study		ABAQUS
	5	10	20	40	60	$\sigma_s = 0$	$\varepsilon_s = 0$	
$[0]_{16}$	152.38	151.06	150.73	150.65	150.63	150.62	151.26	149.68
$[15/-15]_{4S}$	197.15	195.75	195.40	195.31	195.30	195.28	206.82	192.03
$[30/-30]_{4S}$	174.71	173.61	173.33	173.26	173.25	173.24	243.70	167.58
$[45/-45]_{4S}$	112.37	111.67	111.50	111.46	111.45	111.44	194.56	107.24
$[60/-60]_{4S}$	80.12	79.62	79.49	79.46	79.46	79.45	111.13	77.07
$[75/-75]_{4S}$	52.02	51.69	51.62	51.60	51.60	51.59	54.74	50.85
$[90/-90]_{4S}$	31.05	30.85	30.80	30.79	30.79	30.79	30.89	30.62

Table 3 Lateral buckling moments of SS beams with bisymmetric cross-section (Nm)

Lay-ups	Number of finite beam elements, $\sigma_s = 0$					This study		ABAQUS
	5	10	20	40	60	$\sigma_s = 0$	$\varepsilon_s = 0$	
$[0]_{16}$	469.86	449.93	445.20	444.03	443.82	443.64	445.93	439.03
$[15/-15]_{4S}$	497.05	479.36	475.15	474.11	473.92	473.75	508.32	465.01
$[30/-30]_{4S}$	376.90	366.37	363.85	363.23	363.11	363.01	528.66	349.00
$[45/-45]_{4S}$	233.89	227.83	226.38	226.02	225.95	225.90	404.04	215.91
$[60/-60]_{4S}$	166.22	161.94	160.91	160.65	160.60	160.57	227.20	155.17
$[75/-75]_{4S}$	109.34	106.43	105.73	105.56	105.53	105.50	112.27	103.87
$[90/-90]_{4S}$	68.09	66.11	65.64	65.53	65.50	65.48	65.71	65.11

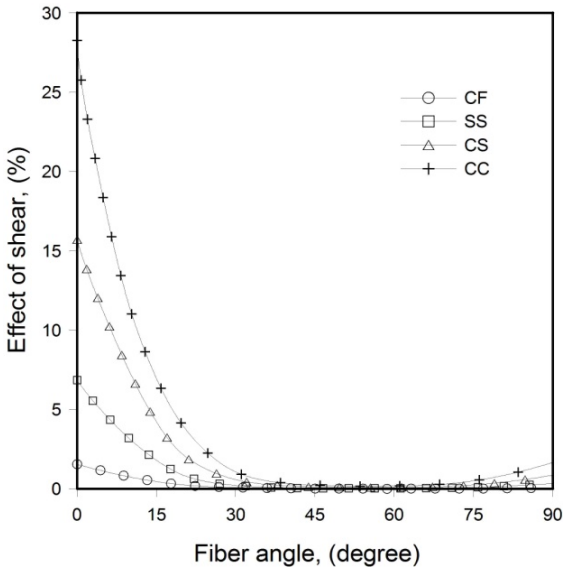

Fig. 4 Effect of shear for bisymmetric I-beams with respect to the fiber angle change, ($L/h = 20$)

those from the present method since the solutions obtained from the Lagrangian interpolation polynomial which satisfies only displacement continuity at nodal point of beam element are approximate. Resultantly, it reveals that at least 40 and 60 finite beam elements are required to achieve the satisfactory results for CF and SS beams, respectively. Whereas, it is possible to obtain the exact results though only a minimum number of beam elements in this study are used.

In order to investigate the effect of shear deformation on the lateral buckling moment, the variation of the effect of shear is plotted in Fig. 4 for beams with $L/h = 20$. The boundary conditions under consideration are CF, SS, CS (clamped-simply), and CC (clamped-clamped) boundary conditions. It can be observed from Fig. 4 that the shear effects are the largest at $\psi = 0°$ and the smallest at $\psi = 50°$ regardless of the boundary conditions. As expected, the shear effect becomes increasing as the end condition of beam is restrained. Fig. 5 shows the shear effects on lateral buckling moment with respect to the various values of the modulus ratio E_1 / E_2 for a CC

beam. It is interesting to observe that the maximum shear effect occurs at $\psi = 45°$ for beam with isotropic material (E_1/E_2=1), while it takes place at $\psi = 0°$ for anisotropic beams. It is noteworthy that for anisotropic beams, the shear effect increases as E_1/E_2 increases in the range of $\psi \leq 18°$. Whereas, it decreases with increase of E_1/E_2 in $\psi > 18°$ and appears to be minimum at $\psi = 52°$. In Fig. 6, for beams which have the $[0]_{16}$ lay-up and E_1/E_2 of 50, the shear effects are presented with respect to the span-to-height ratio L/h. It appears that the laminated composite beam theory considering shear effect is very effective in the region where L/h is less than 80.

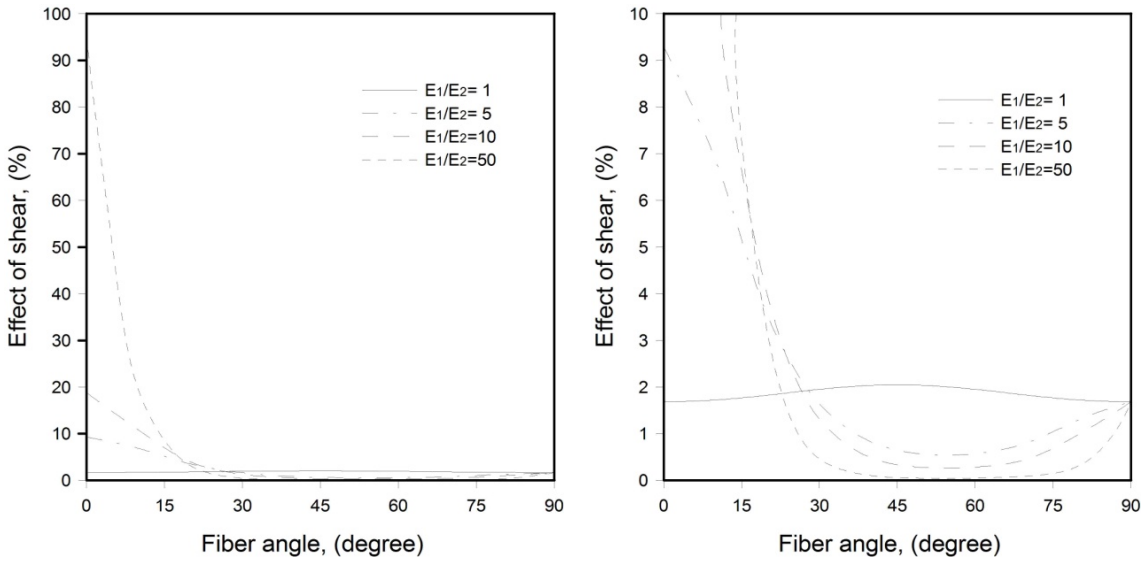

(a) Effect of shear (b) Region of interest

Fig. 5 Effect of shear of the CC bisymmetric I-beams with various modulus ratios, (L/h =20)

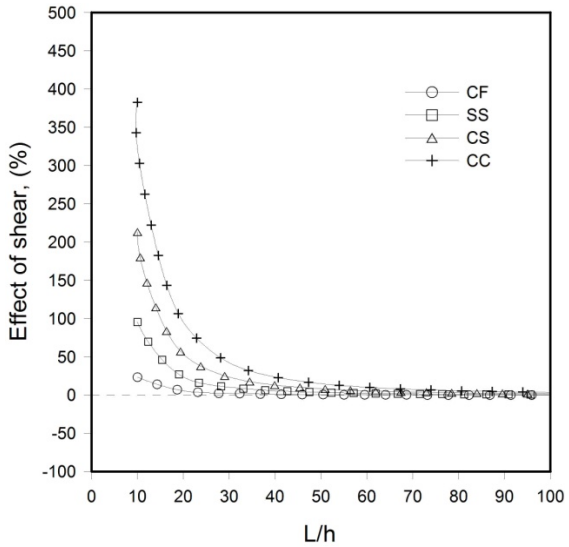

Fig. 6 Effect of shear for beams with $[0]_{16}$ lay-up with respect to the span-to-height ratio, (E_1/E_2 =50)

5.2 Monosymmetric I-beams

In this example, the lateral buckling problems of the monosymmetric I-beams with symmetric and arbitrary lay-ups are concerned. The material used is the same as the previous example. First, for the symmetrically laminated beams with L/h of 40 and b_1 of 15 mm, the lateral buckling moments evaluated by this study are shown in Tables 4 and 5 for CF and SS beams, respectively, together with results from the various values of finite beam elements and those from ABAQUS. It can be found from Tables 4 and 5 that the correlation of the present results based on $\sigma_s = 0$ assumption and the solutions from ABAQUS is seen to be excellent for all lay-ups considered. It can also be observed that considerable numbers of the finite beam elements (at least 40 elements) are needed to obtain the highly accurate results.

In order to investigate the effect of SOCT on the lateral buckling moment for the laminated composite beams with monosymmetic I-shaped cross-section, the relative difference of buckling moment due to SOCT is presented in Fig. 7 for four boundary conditions. In Fig. 7, M_{cr}^{nst} means the critical buckling moment neglecting SOCT in Eq. (21). It is seen that the effect of SOCT is more pronounced for beams with orthotropic lay-up ($\psi = 0°$) and has a minimum value around $\psi = 53°$ for all boundary conditions. It is also seen that as the end boundary condition is restrained, the SOCT effect increases and its value is as much as 45% for a CC beam. Fig. 8 shows the effect of SOCT for SS beams with various values of b_2 / b_1. In this case, the value of b_2 keeps 2.5 mm, while

Table 4 Lateral buckling moments of CF beams with monosymmetric cross-section (Nm)

Lay-ups	Number of finite beam elements, $\sigma_s = 0$					This study		ABAQUS
	5	10	20	40	60	$\sigma_s = 0$	$\varepsilon_s = 0$	
$[0]_{16}$	67.51	67.13	67.03	67.01	67.00	67.00	67.19	69.83
$[15/-15]_{4S}$	114.12	113.51	113.35	113.32	113.31	113.30	118.33	114.34
$[30/-30]_{4S}$	119.42	118.73	118.56	118.52	118.51	118.51	160.43	115.55
$[45/-45]_{4S}$	80.64	80.16	80.05	80.02	80.01	80.00	135.47	77.15
$[60/-60]_{4S}$	57.59	57.24	57.16	57.14	57.13	57.13	79.09	55.57
$[75/-75]_{4S}$	36.46	36.24	36.19	36.18	36.18	36.17	38.38	35.92
$[90/-90]_{4S}$	20.54	20.46	20.43	20.42	20.42	20.42	20.47	20.61

Table 5 Lateral buckling moments of SS beams with monosymmetric cross-section (Nm)

Lay-ups	Number of finite beam elements, $\sigma_s = 0$					This study		ABAQUS
	5	10	20	40	60	$\sigma_s = 0$	$\varepsilon_s = 0$	
$[0]_{16}$	145.15	140.59	139.51	139.24	139.19	139.15	139.68	147.67
$[15/-15]_{4S}$	213.66	208.67	207.47	207.17	207.12	207.08	216.94	211.80
$[30/-30]_{4S}$	226.19	221.23	220.04	219.74	219.68	219.64	292.77	214.19
$[45/-45]_{4S}$	157.85	154.21	153.33	153.11	153.07	153.04	252.38	147.18
$[60/-60]_{4S}$	113.25	110.63	109.99	109.84	109.81	109.79	149.57	106.86
$[75/-75]_{4S}$	70.53	68.95	68.57	68.47	68.45	68.44	72.37	68.42
$[90/-90]_{4S}$	37.78	37.94	37.74	37.69	37.68	37.67	37.77	38.55

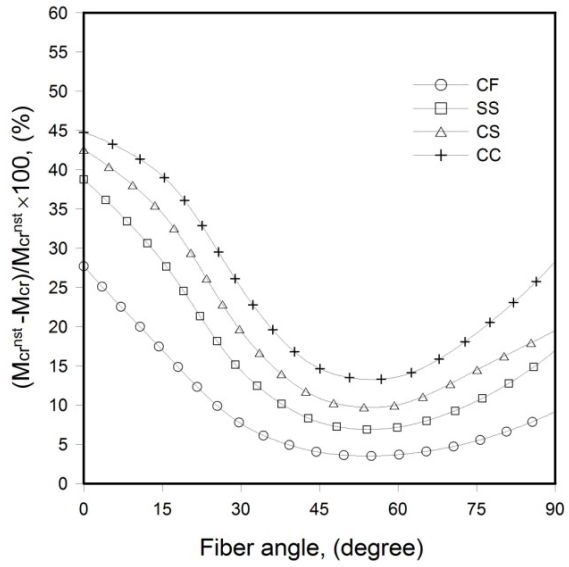

Fig.7 Effect of SOCT for monosymmetric beams with $[\psi / -\psi]_{4S}$ lay-ups, (L/h =40)

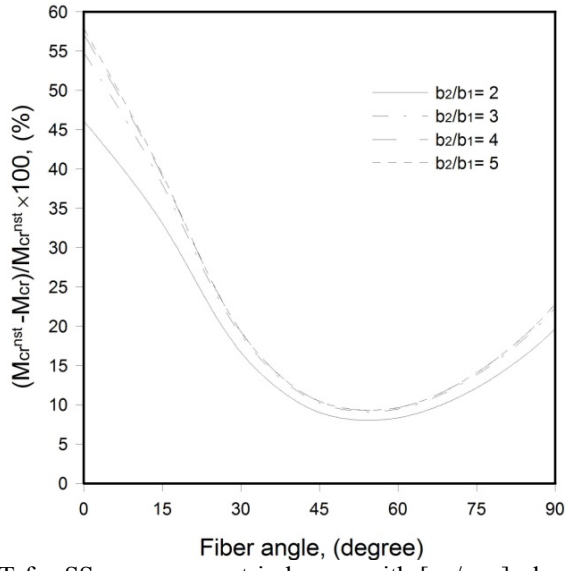

Fig. 8 Effect of SOCT for SS monosymmetric beams with $[\psi / -\psi]_{4S}$ lay-ups and with various values of b_2 / b_1, (L/h =40)

that of b_1 is changed. It is observed that as b_2 / b_1 increases, the SOCT effect increases and does notincrease no longer after $b_2 / b_1 = 5$. To study the influence of span-to-height ratio of beam on the effect of SOCT, the effect of SOCT for beams with $[56/-56]_{4S}$ lay-up is presented in Fig. 9 with respect to the span-to-height ratio. It is seen that the SOCT effect decreases with increase of span-to-height ratio for all boundary conditions.

Finally, to validate the current approach for the lateral buckling analysis of the laminated

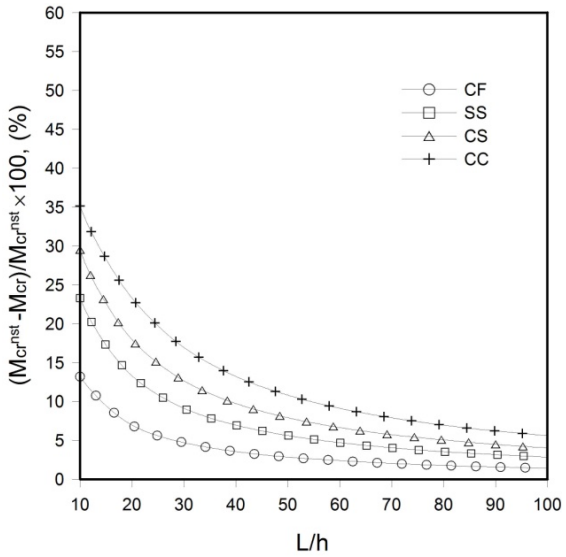

Fig. 9 Effect of SOCT for monosymmetric beams with $[56/-56]_{4S}$ lay-up with respect to the span-to-height ratio

Table 6 Lateral buckling moments of SS beams with monosymmetric cross-section (Nm)

Lay-ups	Number of finite beam elements, $\sigma_s = 0$					This study		ABAQUS
	5	10	20	40	60	$\sigma_s = 0$	$\varepsilon_s = 0$	
[0/30/60/90]	60.20	59.87	59.79	59.77	59.77	59.77	64.09	58.83

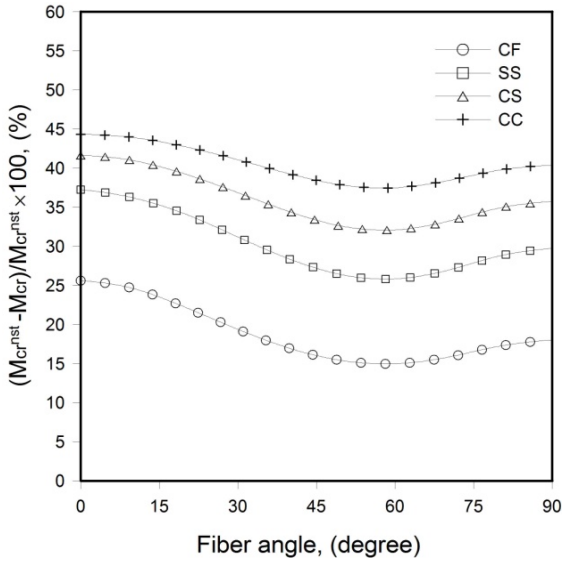

Fig. 10 Effect of SOCT for monosymmetric beams with [0 / ψ / $-\psi$ / 90] lay-ups, (L/h =40)

composite beams with arbitrary lay-up, the monosymmetric I-beam with nonsymmetric lay-up is considered. Four layers of [0/30/60/90] with equal ply thicknesses are used for both flanges and web and the half width of top flange b_1 is chosen by 15 mm. For beams with this lay-up, the extension-shear (A_{16} and A_{26}), bending-twisting (D_{16} and D_{26}), and extension-twisting and bending-shearing (B_{16} and B_{26}) couplings have non-zero values since the lay-up is nonsymmetric with respect to the middle plane of the plate wall. For CF beam with $L/h = 40$, the present critical buckling moment is compared with ABAQUS solution in Table 6. The excellent agreement between results from this study based on $\sigma_s = 0$ assumption and ABAQUS analysis is achieved. Fig. 10 shows the variation of effect of SOCT for monosymmetric beams with $[0 / \psi / -\psi / 90]$ lay-ups with respect to the fiber angle change. The maximum and minimum effects of SOCT are seen to take place at $\psi = 0°$ and 53°, respectively. On the other hand, the difference of SOCT effect with respect to the fiber angle is smaller than that of beams with symmetric lay-ups as shown in Fig. 7.

6. Conclusions

The improved thin-walled laminated composite beam theory considering shear effects due to the shear forces and the restrained warping torsion has been developed for the lateral stability analysis. By using the extended Hamilton's principle, the stability equations and force-displacement relationships are derived and the member stiffness matrix is rigorously evaluated based on the power series expansions of displacement components. In addition, the finite element model, for comparison, using the Lagrangian interpolation polynomial is presented.

Through the numerical examples, the present study is validated comparing the coupled buckling responses with results from other researchers and the finite element solutions using the isoparametric beam elements and the shell elements of ABAQUS. Good correlation is achieved for various beams with bisymmetric and monosymmetric cross-sections, lamination schemes, boundary conditions considered in this study. Based on numerical results, the following conclusions are made

1) The present numerical method using a minimum number of element was capable of predicting the lateral buckling moment for bisymmetric and monosymmetric I-beams with arbitrary lay-ups.
2) For isotropic beams, the maximum shear effect occurs at $\psi = 45°$, whereas it takes place $\psi = 0°$ for anisotropic beams. Moreover, the shear effect increases as E_1 / E_2 increases in the lower range of fiber angle. On the other hand, it decreases with increase of E_1 / E_2 in the higher ranger of one.
3) The effect of the second-order coupling torque is largest for orthotropic beams, while it has a smallest value around $\psi = 53°$ for monosymmetric beams with both symmetric and nonsymmetric lay-ups. Additionally, the second-order coupling torque has a significant role in shorter beams.

It is judged that the present numerical procedure provides a refined method for not only the evaluation of the stiffness matrix of shear deformable laminated composite beams but also general solutions of simultaneous ordinary differential equations of the higher order. This composite beam element also eliminates discretization errors and is free from the shear locking since the displacement state vector satisfies the homogenous form of the simultaneous ordinary differential equations.

Acknowledgements

This work is a part of a research project by Korea Ministry of Land, Transportation Maritime Affairs (MLTM) through Core Research Project 1 of Super Long Span Bridge R&D Center. This research was supported by Basic Science Research Program through the National Research Foundation of Korea (NRF) funded by the Ministry of Education, Science and Technology (2012R1A1A2007054). The authors wish to express their gratitude for the financial support.

References

ABAQUS (2003), *Standard user's manual*, Ver. 6.1, Hibbit, Kalsson & Sorensen Inc.

Abramovich, H., Eisenberger, M. and Shulepov, O. (1996), "Vibration and buckling of cross-ply nonsymmetric laminated composite beams", *AIAA J*., **34**(5), 1064-1069.

Barbero, E.J. (1999), *Introduction to Composite Materials Design*, Taylor & Francis.

Bathe, K.J. (1996), *Finite Element Procedures*, Prentice-Hall, Englewood Cliffs, NJ, USA.

Cortínez, V.H. and Piovan, M.T. (2006), "Stability of composite thin-walled beams with shear deformability", *Comput*. *Struct*., **84**(15-16), 978-990.

Gunnlaugsson, G.A. and Pedersen, P.T. (1982), "A finite element formulation for beams with thin-walled cross- sections", *Comput*. *Struct*., **15**(6), 691-699.

Kabir, M.Z. and Sherbourne, A.N. (1998), "Optimal fibre orientation in lateral stability of laminated channel section beams", *Compos*. *Part B*, **29**(1), 81-87.

Kim, M.Y., Chang, S.P. and Kim, S.B. (1994), "Spatial stability and free vibration of shear flexible thin-walled elastic beams", *Int*. *J*. *Numer*. *Meth*. *Eng*. **37**(23), 4117-4140.

Kim, N.I., Shin, D.K. and Kim, M.Y. (2007), "Improved flexural-torsional stability analysis of thin-walled composite beam and exact stiffness matrix", *Sci*. **49**(8), 950-969.

Kollár, L.P. and Springer, G.S. (2003), *Mechanics of Composite Structures*, Cambridge University Press.

Lee, J.H. (2006), "Lateral buckling analysis of thin-walled laminated composite beams with monosymmetric sections", *Eng*. *Struct*., **28**(14), 1997-2009.

Lee, J., Kim, S.E. and Hong, K. (2002), "Lateral buckling of I-section composite beams", *Eng*. *Struct*., **24**(7), 955-964.

Lin, Z.M., Polyzois, D. and Shah, A. (1996), "Stability of thin-walled pultruded structural members by the finite element method", *Thin-Walled Struct*., **24**(1), 1-18.

Machado, S.P. and Cortínez, V.H. (2005), "Non-linear model for stability of thin-walled composite beams with shear deformation", *Thin-Walled Struct*., **43**(10), 1615-1645.

Mathematica (2009), *Wolfram Mathematica 7*, Wolfram Research Inc., IL, USA.

Piovan, M.T., Filipich, C.P. and Cortínez, V.H. (2008), "Exact solutions for coupled free vibrations of tapered shear-flexible thin-walled composite beams", *J*. *Sound Vib*., **316**(1-5), 298-316.

Qiao, P., Zou, G. and Davalos, J.F. (2003), "Flexural-torsional buckling of fiber-reinforced plastic composite cantilever I-beams", *Compos*. *Struct*., **60**(2), 205-217.

Sapkás, A. and Kollár, L.P. (2002), "Lateral-torsional buckling of composite beams", *Int*. *J*. *Solids Struct*., **39**(11), 2939-2963.

Shield, C.K. and Morey, T.A. (1997), "Kinematic theory for buckling of open and closed section thin-walled composite beams", *J*. *Eng*. *Mech*., **123**(10), 1070-1081.

Smith, E.C. and Chopra, I. (1991), "Formulation and evaluation of an analytical model for composite box beams", *J*. *Am*. *Helicopter Soc*., **36**(3), 23-35.

Wendroff, B. (1966), *Theoretical Numerical Analysis*, Academic Press, NY, USA.

Zhen, W. and Wanji, C. (2008), "An assessment of several displacement-based theories for the vibration and stability analysis of laminated composite and sandwich beams", *Compos*. *Struct*., **84**(4), 337-349.

CC

Appendix: Detailed expressions of the laminate stiffnesses E_{ij}

$$
\begin{aligned}
E_{11} &= \int_A \overline{Q}_{11}^{*}\, dydz \\
E_{12} &= \int_A \overline{Q}_{11}^{*}\,(z-\eta\cos\psi)dydz \\
E_{13} &= \int_A \overline{Q}_{11}^{*}\,(y+\eta\sin\psi)dydz \\
E_{14} &= \int_A \overline{Q}_{11}^{*}(\phi+\eta q)dydz \\
E_{15} &= \int_A \overline{Q}_{16}^{*}\eta\, dydz \\
E_{16} &= \int_A \overline{Q}_{16}^{*f}\, dydz \\
E_{17} &= \int_A \overline{Q}_{16}^{*w}\, dydz \\
E_{18} &= \int_A \left[\overline{Q}_{16}^{*w}(y-e_2)-\overline{Q}_{16}^{*f}(z-e_3)\right]dydz \\
E_{22} &= \int_A \overline{Q}_{11}^{*}\left(z^2-2z\eta\cos\psi+\eta^2\cos^2\psi\right)dydz \\
E_{23} &= \int_A \overline{Q}_{11}^{*}\left(yz-y\eta\cos\psi+z\eta\sin\psi-\eta^2\sin\psi\cos\psi\right)dydz \\
E_{24} &= \int_A \overline{Q}_{11}^{*}\left(\phi z-\phi\eta\cos\psi+z\eta q-\eta^2 q\cos\psi\right)dydz \\
E_{25} &= \int_A \overline{Q}_{16}^{*}\left(z\eta-\eta^2\cos\psi\right)dydz \\
E_{26} &= \int_A \overline{Q}_{16}^{*f}\,(z-\eta\cos\psi)dydz \\
E_{27} &= \int_A \overline{Q}_{16}^{*w}\,(z-\eta\cos\psi)dydz \\
E_{28} &= \int_A \left[\overline{Q}_{16}^{*w}(y-e_2)-\overline{Q}_{16}^{*f}(z-e_3)\right](z-\eta\cos\psi)dydz \\
E_{33} &= \int_A \overline{Q}_{11}^{*}\left(y^2+2y\eta\sin\psi+\eta^2\sin^2\psi\right)dydz \\
E_{34} &= \int_A \overline{Q}_{11}^{*}\left(\phi y+\phi\eta\sin\psi+y\eta q+\eta^2 q\sin\psi\right)dydz \\
E_{35} &= \int_A \overline{Q}_{16}^{*}\left(y\eta+\eta^2\sin\psi\right)dydz \\
E_{36} &= \int_A \overline{Q}_{16}^{*f}\,(y+\eta\sin\psi)dydz
\end{aligned}
$$

$$
\begin{aligned}
E_{37} &= \int_A \overline{Q}_{16}^{*w}\left(y+\eta\sin\psi\right)dydz \\
E_{38} &= \int_A \left[\overline{Q}_{16}^{*w}\left(y-e_2\right)-\overline{Q}_{16}^{*f}\left(z-e_3\right)\right]\left(y+\eta\sin\psi\right)dydz \\
E_{44} &= \int_A \overline{Q}_{11}^{*}\left(\phi^2+2q\eta\phi+q^2\eta^2\right)dydz \\
E_{45} &= \int_A \overline{Q}_{16}^{*}\left(\phi\eta+q\eta^2\right)dydz \\
E_{46} &= \int_A \overline{Q}_{16}^{*f}\left(\phi+q\eta\right)dydz \\
E_{47} &= \int_A \overline{Q}_{16}^{*w}\left(\phi+q\eta\right)dydz \\
E_{48} &= \int_A \left[\overline{Q}_{16}^{*w}\left(y-e_2\right)-\overline{Q}_{16}^{*f}\left(z-e_3\right)\right]\left(\phi+q\eta\right)dydz \\
E_{55} &= \int_A \left(\overline{Q}_{66}^{*f}\eta^2\cos\psi+\overline{Q}_{66}^{*w}\eta^2\sin\psi\right)dydz \\
E_{56} &= \int_A \overline{Q}_{66}^{*f}\,\eta\cos\psi\,dydz \\
E_{57} &= \int_A \overline{Q}_{66}^{*w}\,\eta\sin\psi\,dydz \\
E_{58} &= \int_A \left[\overline{Q}_{66}^{*w}\left(y-e_2\right)\eta\sin\psi-\overline{Q}_{66}^{*f}\left(z-e_3\right)\eta\cos\psi\right]dydz \\
E_{66} &= \int_A \overline{Q}_{66}^{*f}\,dydz \\
E_{68} &= -\int_A \overline{Q}_{66}^{*f}\left(z-e_3\right)dydz \\
E_{77} &= \int_A \overline{Q}_{66}^{*w}\,dydz \\
E_{78} &= \int_A \overline{Q}_{66}^{*w}\left(y-e_2\right)dydz \\
E_{88} &= \int_A \left[\overline{Q}_{66}^{*f}\left(z-e_3\right)^2+\overline{Q}_{66}^{*w}\left(y-e_2\right)^2\right]dydz
\end{aligned}
\qquad \text{(A-1)}
$$